processes

MDPI

Article

Solarized Auger Reactor for Organic Waste Upgrading Through Pyrolysis

Ernesto Anguera Romero [1,*], Nidia Aracely Cisneros-Cárdenas [2], Arturo Aspiazu-Méndez [1], Heidi Isabel Villafán Vidales [1], Pablo Pizarro Medina [3] and Claudio A. Estrada [1]

[1] Instituto de Energías Renovables, Universidad Nacional Autónoma de México, Temixco 62588, Morelos, Mexico; arasm@ier.unam.mx (A.A.-M.); hivv@ier.unam.mx (H.I.V.V.); cestrada@ier.unam.mx (C.A.E.)
[2] Departamento de Ingeniería Química y Metalurgia, Facultad Interdisciplinaria de Ingeniería, Universidad de Sonora, Hermosillo 83000, Sonora, Mexico; aracely.cisneros@unison.mx
[3] Green Oil Energy Systems SLP, Travesía de la Cruz Verde 2, 45002 Toledo, Spain; pizarro.medina@gmail.com
* Correspondence: eranr@ier.unam.mx

Abstract

This study reports the initial thermal and thermochemical performance of a novel solarized Auger-type reactor for Pyrolysis (SARP), specifically developed for the valorization of organic solid waste into solar-derived fuels. A key innovation of this system lies in its integration with a high-flux, point-focus solar concentrator that enables controlled delivery of concentrated solar radiation to drive endothermic processes. At the front of the reactor, the thermal evaluation under solar irradiation shows that surface temperatures reached up to approximately 750 °C on the exterior, while the hottest section of the interior briefly reached approximately 700 °C, in the pyrolysis zone. In contrast, the preheating zone inside the reactor exhibits temperatures ranging from 160 °C to 306 °C, indicating a non-uniform thermal profile for the incoming feedstock. The campaign focused on thermochemical pyrolysis, in which pecan walnut tree pruning residue biomass was processed under controlled semicontinuous operation. Batches of 600 g were pyrolyzed, yielding approximately 390 g of biochar and achieving a peak hydrogen concentration of 14.5% vol in the product gases. These findings demonstrate the reactor's potential for solar-driven waste-to-fuel conversion.

Keywords: solar thermochemical conversion; screw reactor; screw reactor; solarized auger reactor; waste-to-fuel conversion

check for updates

Academic Editor: Yi-Kuo Chang

Received: 3 September 2025
Revised: 28 September 2025
Accepted: 5 October 2025
Published: 9 October 2025

Citation: Anguera Romero, E.; Cisneros-Cárdenas, N.A.; Aspiazu-Méndez, A.; Villafán Vidales, H.I.; Pizarro Medina, P.; Estrada, C.A. Solarized Auger Reactor for Organic Waste Upgrading Through Pyrolysis. *Processes* **2025**, *13*, 3216. https://doi.org/10.3390/pr13103216

Copyright: © 2025 by the authors. Licensee MDPI, Basel, Switzerland. This article is an open access article distributed under the terms and conditions of the Creative Commons Attribution (CC BY) license (https://creativecommons.org/licenses/by/4.0/).

1. Introduction

Lignocellulosic biomass is considered one of the most important renewable energy sources [1]. Its energy value can be enhanced through thermochemical treatments such as pyrolysis, gasification, and thermal liquefaction. In particular, the pyrolysis of organic residues requires specific operating conditions, including high temperatures and non-oxidative atmosphere. Typically, the energy supply is derived from the combustion of raw material itself, in electric solar furnaces, microwaves, and to a lesser extent, from renewable sources.

Pyrolysis offers advantages over other treatments due to its processing times and commercial appeal, despite current technological challenges [2]. This reaction yields three fractions which are solid, liquid, and gaseous, all of which are of interest for diverse applications. The solid fraction, biochar, is used for soil remediation and improvement,

carbon sequestration, additive in organic solid waste composing, and for water and wastewater decontamination, among others [3]. The liquid fraction, or bio-oil, originates from the condensable vapors during pyrolysis at environmental temperature. Bio-oil has emerged as a promising alternative to crude oil, with several advantages such as CO_2/GHG-neutral emissions, absence of SOx, and the possibility of renewable local production, in contrast to conventional fuels [4]. The gaseous fraction, or syngas, holds high energetic potential and may address issues related to energy storage and transport [5,6].

A considerable number of studies on the pyrolysis of organic residues have been reported, addressing different aspects such as reaction kinetics, feedstock type, residence time, operating temperature, and reactor configurations. This study conducts a systematic comparison of the literature on auger reactors with different energy sources, with particular emphasis on solar-powered systems. The analysis reported in Table 1 considers energy sources, feedstock type, operating temperatures, system scale, and product yields. In addition, the previously published studies about auger reactors and solar-powered systems are analyzed as a part of this comparison.

Campuzano et al. [7] published a review article on auger reactors for the pyrolysis of organic residues, considering various factors such as reactor design, screw configuration, biomass type, and thermal energy supply. From this study, 30 auger reactors were reviewed, and the distribution by type of energy supply is presented in Figure 1. The predominant energy source reported in this study was electric resistance heating.

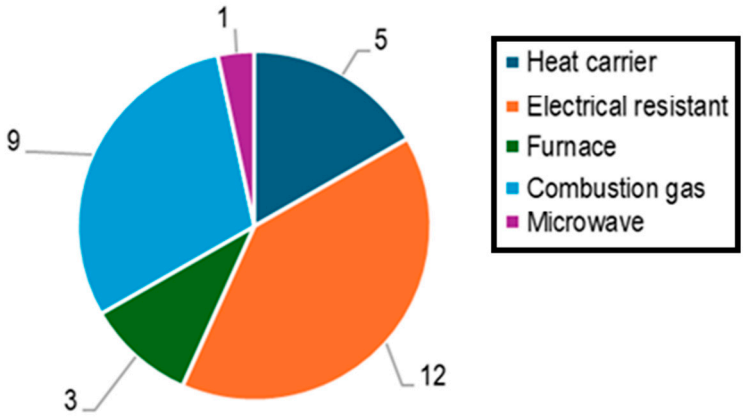


Figure 1. Distribution by type of energy supply from Campuzano et al. [7].

Table 1. Summary of the reported literature on auger reactors for pyrolysis.

Ref.	Scale	Energy Source	Feedstock	Temperature (°C)	Product Yield (%)		
					Biochar	Tar	Gas
[1]	Laboratory	Electricity	Saw dust	350–550	19	57	24
[8]	Laboratory	Heat solid carriers	Sawdust and bagasse	500	-	-	-
[9]	Laboratory	Microwaves	Red wood waste and textile dyeing sludge	450–750	65–50	20–18	15–40
[10]	Laboratory	Microwaves	Wood waste	550	-	-	-
[11]	Industrial	Flue gas	Elephant grass	400–600	35–26	27–30	35–45
[12]	Laboratory	Flue gas	Palm oil waste	450–750	-	-	-
[13]	Laboratory	Electricity	Flax shive	500–700	86–46	3–2	10–31
[14]	Pilot	Electricity	Cogon grass	400–500	32–24	27–21	-
[15]	Laboratory	Electricity	Mustard	500	33	51	16
[16]	Industrial	Electricity	Cane bagasse	450–550	13–15	40–70	46–14
[17]	Laboratory	Electricity	Wood	300–900	54–19	34–11	10–70
[18]	Industrial	Electricity	Pine nut shell	300–700	52–27	31–39	16–41
[19]	Laboratory	Electricity	Pine sawdust	400–600	38–22	20–21	28–37
[20]	Laboratory	Electricity	Pine sawdust	700–900	30–20	20–10	50–74
[21]	Laboratory	Electricity	Coffee grounds	350–550	27–18	21–14	27–45
[22]	Laboratory	Electricity	Sugarcane bagasse	400–600	27–17	30–22	-
[23]	TLR-5	Electricity	Rice husk	850	35	8	39

The authors conducted a literature review of studies reported after 2019, summarized in Table 1. The analysis focused on the type of energy supply, identifying electricity as the most common, followed by flue gas and microwaves. Most reactors were operated at laboratory scale, with few industrial scales reported. Operating temperatures typically ranged between 400 and 550 °C, with some exceptions at significantly higher values [23].

Some authors describe pyrolysis as a sustainable process, since its own products can compensate for the energy demand of the plant [24]. However, only a limited number of studies address the use of renewable energy to satisfy its energy demand, compared to the extensive research available on pyrolysis. Maytorena et al. [25] reviewed the state of the art in solar-driven pyrolysis, where energy demand was supplied by concentrated technologies. Their review highlighted advances and challenges of this synergy. This report also includes studies employing solar simulators as the energy source. The distribution by type of concentrated technology is as follows: 39% parabolic dish, 30% solar simulator, 17% solar furnace, 9% Fresnel lens, and 4% parabolic through. Reported solar reactor types included fixed bed (61%), batch (33%), and tubular reactor (6%), all at laboratory scale. Despite successful industrial cases such as Synhelion [26], major technological challenges remain, particularly in scalability and industrial deployment.

Zeng et al. [27] investigated beech wood pyrolysis in a fixed bed reactor heated by a solar furnace. The biomass, with high volatile content (~85 wt.%) and low moisture (~6 wt.%) was directly irradiated with concentrated solar energy in an argon rich atmosphere at 600–2000 °C. Product yields were reported as 15–8 wt.% biochar, 63–35 wt.% tar, and 20–62 wt.% gas, with heating rates of 10–450 °C min^{-1}, highlighting precise laboratory control.

Aspiazu et al. [28] examined walnut shell pyrolysis (~80 wt.% volatiles, ~7 wt.% moisture) in a fixed bed reactor indirectly heated with a solar simulator under argon at 380–670 °C, obtaining product distributions of 41–28 wt.% biochar, 49–53 wt.% tar, and 9–18 wt.% gas.

This review compares reported auger reactors by energy source and highlights the absence of documented solar powered devices, underscoring the novelty of solarized auger reactors. To the best of the author's knowledge, research on solar powered auger reactors remains scarce. To address this, the research team designed and tested an uncommon reactor solar driven auger system. This article reports its initial thermochemical performance using walnut tree pruning residues as feedstock for biochar production.

The Solarized Auger Reactor for Pyrolysis (SARP), developed at the Renewable Energy Institute in collaboration with Green Oil Energy Systems, was designed, constructed, and is currently being evaluated within the framework of the DGAPA-UNAM PAPIIT AG-101525 project. This project aims to establish a sustainable process under real and reproducible operating conditions, enabling the production of solar fuels and offering an alternative pathway for organic solid waste management. The integration of concentrated solar energy with biomass provides economic, social, and environmental benefits. Furthermore, the conversion of organic solid waste into solar fuels through concentrated solar energy can be considered a form of chemical storage of renewable energy.

2. Experimental Setup

2.1. Solarized Auger Reactor for Pyrolysis from IER-UNAM

The Solarized Auger Reactor for Pyrolysis from IER is an auger reactor designed for the pyrolysis of organic solid waste (Figure 2).

The SARP is equipped with an internal screw conveyor driven by a chain mechanism coupled to an electrical motor. The screw transports the feedstock from the low temperature zone, located beneath the feedstock system, to the high temperature zone, situated near to a volumetric receiver and above the biochar depot. On the opposite side of the biochar depot, the condensation system is located, comprising a tar filter, a bio-oil outlet, two condensers,

and a syngas collection line linked to an online gas chromatography. Inert gas inlets are provided at both the feed hopper and the biochar depot to maintain a non-oxidizing atmosphere.

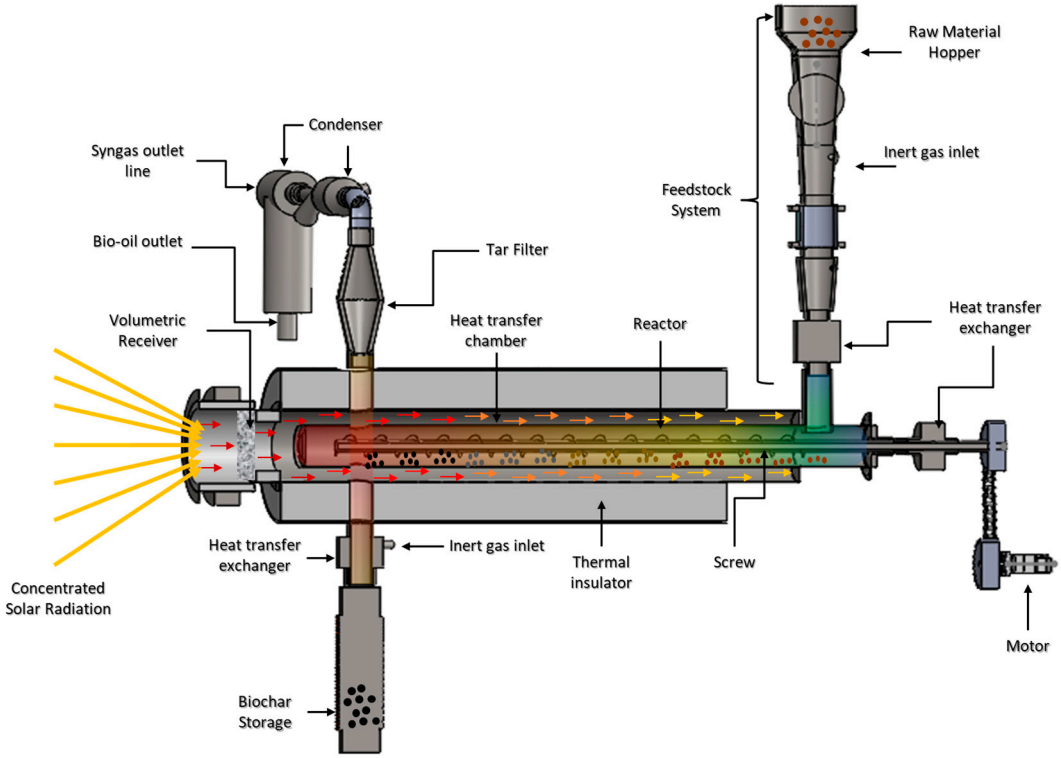


Figure 2. Schematic representation of the SARP reactor, showing the volumetric receiver, feedstock system, screw conveyor, heat transfer units, and outlets for syngas, bio-oil, and biochar. Yellow arrows on the left indicate concentrated solar radiation, while red arrows around the reactor show regions of higher air temperatures using a turbo colormap. Brown circles represent raw biomass, and black circles denote biochar.

Thermal energy is supplied indirectly through a concentric tube heat exchanger composed of three concentric cylinders. The first cylinder (reactor) houses the screw conveyor and is equipped with external fins to enhance heat transfer. The second cylinder (heat transfer chamber), concentric to the first, conducts high temperature air. The heat transfer fluid flows countercurrent respect to the feedstock motion. The third cylinder, concentric to the second, contains thermal insulation.

The heat transfer fluid is atmospheric air, which is heated as it flows through a volumetric receiver positioned in front of the reactor. The receiver absorbs concentrated solar radiation delivered by a solar furnace. After leaving the receiver volume, the heated air circulates through the heat transfer chamber, transferring thermal energy to the reactor.

The temperature control method inside the reactor is achieved by regulating the concentrated radiative flux from the solar furnace using a shutter.

2.2. Solar Furnace from IER-UNAM

The SARP was tested at the Solar Furnace of the Institute of Renewable Energies (HoSIER). The facility includes an 81 m^2 heliostat that directs solar radiation to a concentrator of 409 hexagonal facets with spherical curvature, with a focal length of 3.85 m (Figure 3).

The reactor was mounted on the experimental platform, with its front face placed and centered at the focal point and the housing aligned with the optical axis of the concentrator.

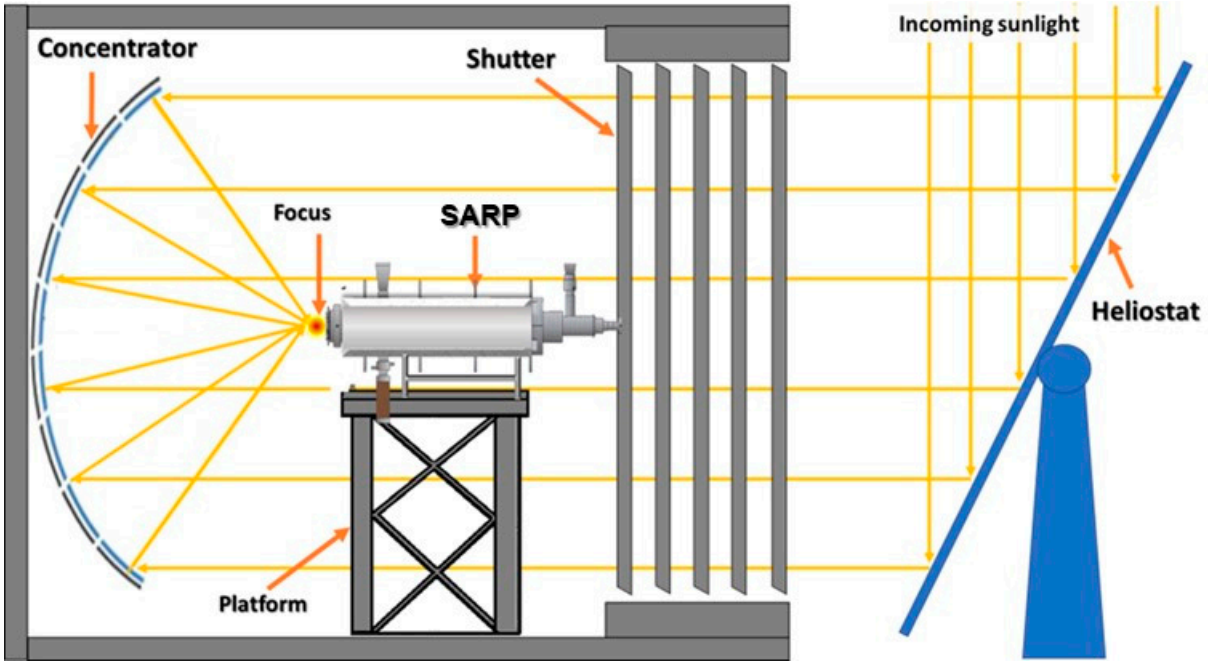


Figure 3. Schematic diagram of the HoSIER components and the location of SARP in the facilities.

Radiative flux on the volumetric receiver was controlled by a vertical curtain attenuator (Shutter) located between the heliostat and the platform; this system allows stabilization of the reactor temperature according to the reaction requirements and climatic conditions, and it enables partial or total blocking of the incident radiative energy for conditioning tests or as a safety measure in the event of unforeseen circumstances or component failures.

Figure 4 presents a photograph of the SARP installation at HoSIER, allowing for visual identification of the main components previously described. The solar concentrator, with its large array of spherical mirrors, and the shutter (attenuator) are both clearly visible. The shutter is positioned to regulate the solar flux that is reflected from the heliostat (not in view) toward the reactor's volumetric receptor.

On the other hand, the reactor system consists of the SARP reactor installed on the optical axis, the biomass feedstock inlet for introducing agroindustrial residues, the motor that drives the screw conveyor, and the biochar storage unit for collecting the solid product. The syngas outlet enables extraction of the gaseous products. The vacuum pump is used to force air through the volumetric receiver, thereby increasing the inlet temperature. The data acquisition system controls the movement and speed of the auger motor, while also monitoring and recording signals from temperature, pressure, and irradiance sensors throughout the experiments.

On a clear day, with the shutter fully open (100%), the concentrated solar radiation incident on a volumetric receiver located at the focal plane can raise its temperature to nearly 2000 °C. Reactor temperature can be controlled by two strategies: adjusting the attenuator aperture or varying the suction rate of the vacuum pump. However, to regulate the temperature at the center of the volumetric receiver while maintaining a fully open attenuator, it is necessary either to increase the distance between the receiver and the focal region by displacing the entire system along the optical axis, or to incorporate a secondary optical element that homogenizes the concentrated solar radiation delivered by the HoSIER.

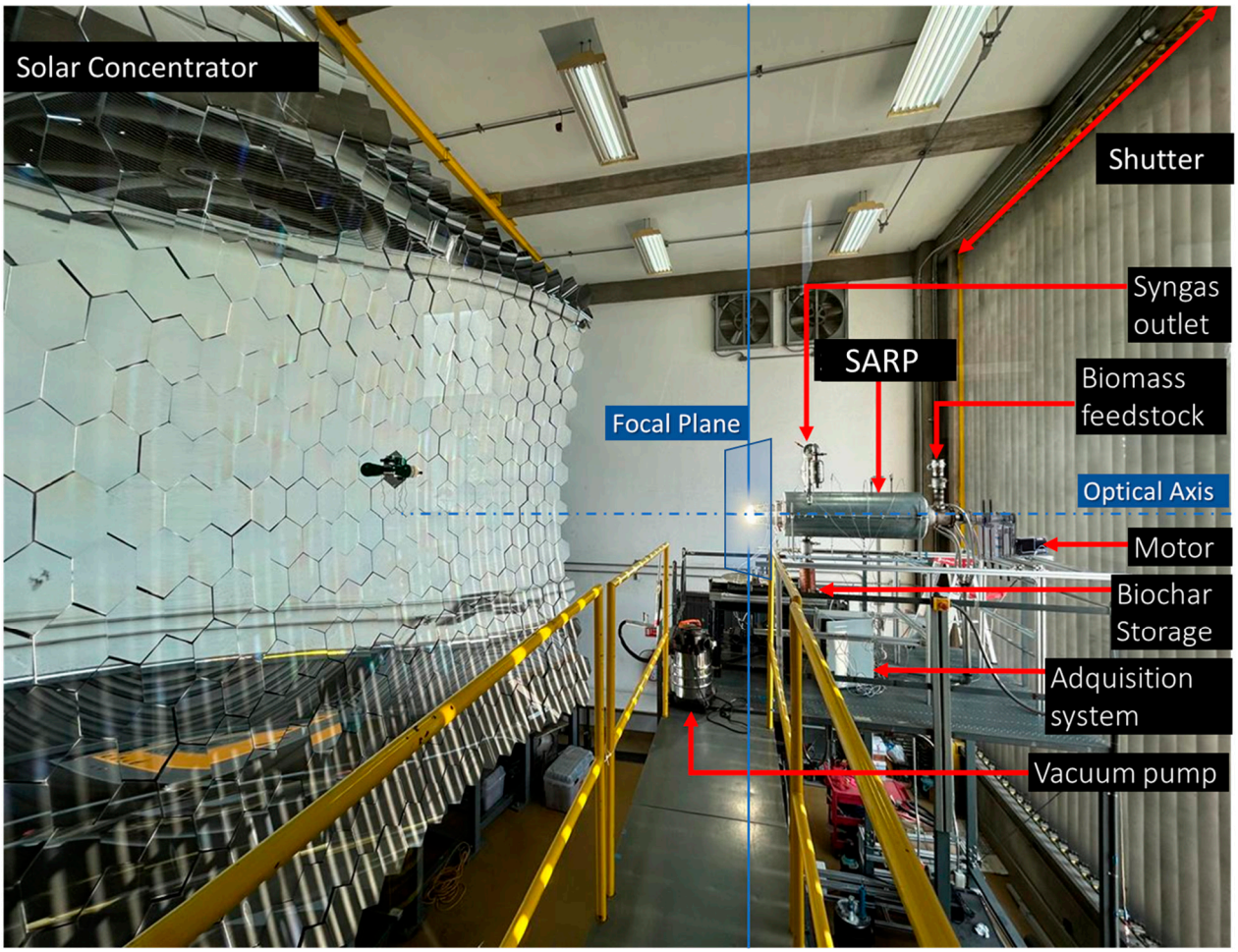


Figure 4. SARP operating in the HoSIER facility. Left: hexagonal mirrors of the HoSIER solar concentrator. Center: SARP system with its main components. Right: shutter partially opened at 20% aperture.

3. Materials and Methods

3.1. Materials

The raw material used for pyrolysis experiments was woody pruning of the tree *Carya illinoinensis*, commonly called pecan walnut (pecan tree). These residues come from pecan nut fields in the state of Sonora, Mexico.

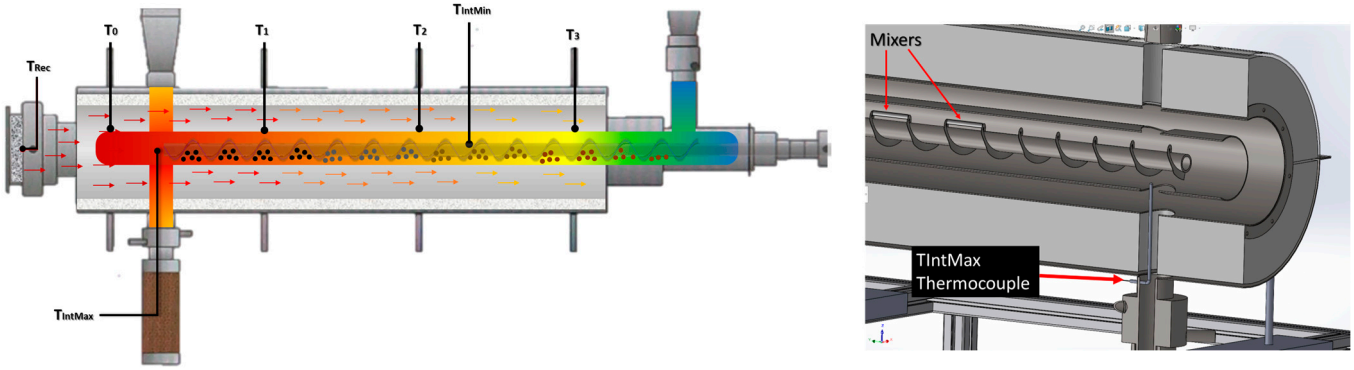
The characterization of this biomass was performed with several analyses. The proximal analysis was carried out using ASTM method E870-82 (2019) [29]. The ultimate analysis was performed with Perkin Elmer (PE2400) equipment (Shelton, CT, USA). Bulk density was determined by ISO 17828:2015 [30]. The higher heating value (HHV) was obtained with the method developed by Channiwala [31]. In addition, as part of this characterization, the thermogravimetric analysis (TGA) was performed using a Discovery TGA 500 equipment (Waters TA Instruments, New Castle, DE, USA), in which the sample was subjected to a temperature of 45 to 900 °C in an atmosphere of nitrogen. The amount of ash was determined by NREL/TP-510-42622 [32].

3.2. Solar Pyrolysis

For the solar pyrolysis procedure, the SARP was instrumented with temperature sensors placed in different zones to enable process control and monitoring. Four main stages were defined for the methodological development, which are described in this section.

3.2.1. Temperature Monitoring and Controlling

For the instrumentation, seven type K thermocouples were installed: two inside the reactor (T_{IntMax} and T_{IntMin}) and five at strategic points of the SARP. To monitor the heat flux input, a thermocouple was placed at the outlet of the volumetric receiver (T_{Rec}). Thermocouples T_0, T_1, T_2, and T_3 recorded axial temperature distribution on the external cylinder housing of the concentric-cylinder heat exchanger. The position and distribution of all thermocouples are shown in Figure 5a.



(**a**) (**b**)

Figure 5. Diagram of thermocouples distribution in the SARP. (**a**) Distribution of thermocouples along the system, (**b**) T_{IntMax} thermocouple position inside the reactor.

The internal thermocouples (T_{IntMax} and T_{IntMin}) have different functions and locations, as shown in Figure 5. T_{IntMax} is located near the focal zone and monitors the maximum biomass temperature during experimentation, and it is considered the closest value for measuring pyrolysis bet temperature; this value is used to define a threshold temperature for activating the transport mechanism and senses the temperature in the pyrolysis zone (see Figure 5b). T_{IntMin} indicates the temperature at the preheating zone which is located at posterior part of the reactor where the biomass is being fed during the experiments.

The external thermocouples (T_0, T_1, T_2 and T_3) monitored the reactor operating temperature to ensure the integrity of the device. The T_{Rec} sensor monitors the air temperature at the outlet of the volumetric receiver and enables the regulation of the solar radiation input to the concentrator through manipulation of the HoSIER shutter.

3.2.2. Stage I: Biomass Preparation and Loading

Before feeding organic matter into SARP, the particle size was homogenized according to the optimal range of 1–5 mm, which favors the transport mechanism. For the experiment, a particle size mixture was used, with 25% below the optimal size and the remaining within the established interval (Figure 6). A total of 600 g of woody pruning residues from *Carya illinoinensis* (walnut tree) was introduced, divided into six equal loads at 3 min intervals, with the screw operating at 0.5 rpm.

3.2.3. Stage II: System Preheating

Preheating was performed by opening the HoSIER shutter, irradiating the volumetric receiver until the threshold temperature (T_{intMax}) of 600 °C was reached, which took 40 min. During this stage, the reactor atmosphere was purged with an inert gas flow, ensuring non-oxidative conditions as confirmed by chromatographic analysis.

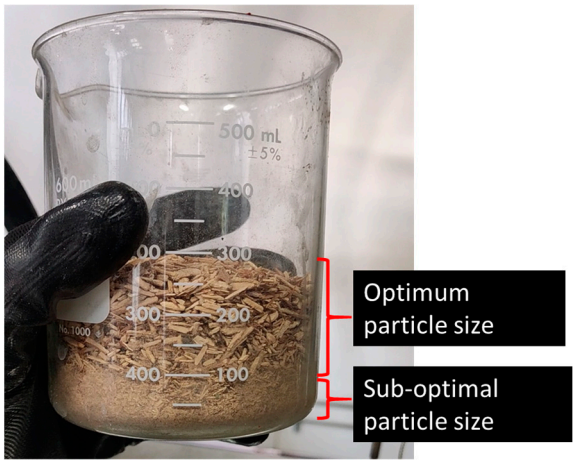


Figure 6. Raw material mix distribution.

3.2.4. Stage III: Pyrolysis

Once the threshold temperature was reached, biomass feeding was activated with the screw set at 0.5 rpm. Under these conditions, pyrolysis was promoted for approximately 100 min. During the process, the inert gas (Argon) flow rate was kept constant at 1.5 L·min^{-1} to maintain a non-oxidative atmosphere.

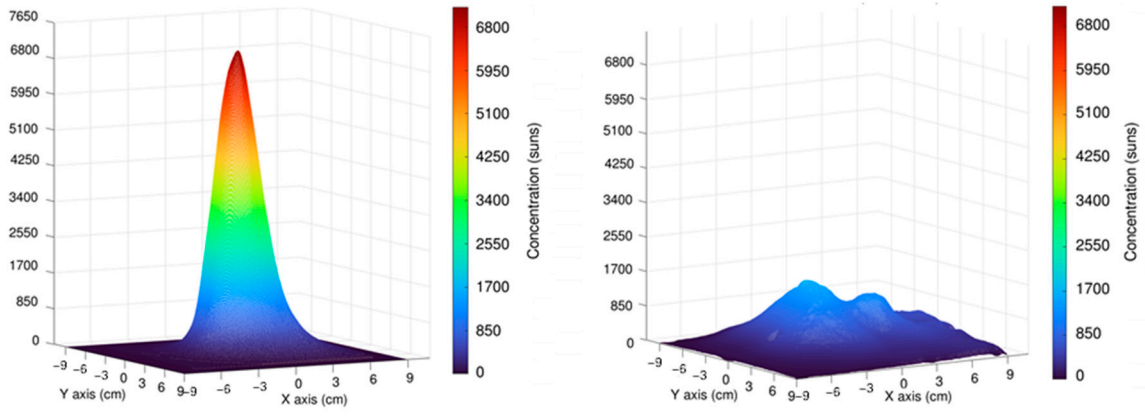
3.2.5. Stage IV: Reactor Cooling and Biochar Collection

After completion of the pyrolysis stage, the HoSIER shutter was fully closed, allowing the system to cool down. Biochar collection was initiated once T_{intMin} reached environmental temperature.

4. Results

4.1. Solar Furnace Characterization

On a clear day (DNI = 1000 W/m^2), the solar radiation concentrated by the HoSIER at the focal zone reaches a peak flux intensity of 6800 suns (Figure 7a), concentrated at the center of the receiver. Under this distribution, however, the central region of the SARP volumetric receiver reaches its melting temperature, causing the porous surface to degrade and obstruct the air channels required for heat transfer from the receiver to the reactor interior. This effect reduces the overall thermal efficiency of the system during operation under optimal solarimetric conditions, when the HoSIER attenuator is fully open.



(**a**) (**b**)

Figure 7. Distribution of the radiative flux concentrated by the HoSIER. (**a**) At the focal plane, (**b**) 8 cm away from the focal plane.

To enable operation at maximum furnace power, the SARP receiver was repositioned 8 cm away from the focal plane, identified as the optimal distance for complete radiative flux entry into the reactor. At this position, the flux distribution (Figure 7b) of the concentrated solar radiation is spread over a circular area in diameter of 18 cm, while the peak flux intensity decreases from 6800 to 1600 suns. This configuration allows reactor operation at the maximum capacity of the HoSIER with the attenuator fully open, while preserving the structural integrity of the volumetric receiver.

4.2. Physicochemical Characterization of Raw Material

Table 2 presents the results of proximate and ultimate analyses for the pruning of *Carya illinoinensis*. The high percentage of volatiles in the sample predicts a high production of condensable vapors, while it is expected to obtain a low production of biochar. It was also found that the raw material has a low percentage of ash (below 3%). On the other hand, high percentages of C and O in elemental analysis predict that it is suitable to obtain a fuel with a high energy value.

Table 2. Ultimate and proximal analysis for *Carya illinoinensis* tree pruning.

Proximal Analysis (Dry Basis)	Weight Percentage (%)	Ultimate Analysis (Dry Basis)	Weight Percentage (%)
Moisture	6.81	C	45.28
Ashes	2.97	H	5.75
Volatiles	69.09	O	47.91
Fixed carbon	21.13	N	1.06

In addition, Table 3 shows the biomass characterization parameters of the raw material, as well as the particle size defined for this study.

Table 3. Granulometry properties and apparent density of *Carya illinoinensis* tree pruning.

Properties	Value
Particle diameter (mm)	1–4
HHV (MJ/kg)	17.55
Apparent density (kg/m^3)	220

Figure 8 shows the results of thermogravimetric analysis (TGA), performed with a heating ramp of 10 °C/min under controlled nitrogen atmosphere. The derivative thermogravimetric (DTG) curve distinguishes three main stages: sample drying, active pyrolysis and passive pyrolysis. Drying occurs in the temperature range of 50 to 150 °C and corresponds to the removal of moisture contained in the sample. Active pyrolysis is associated with the thermal degradation of hemicellulose and cellulose, showing a significant loss of mass in the DTG between 200 and 400 °C, with a maximum peak around 329 °C. Finally, passive pyrolysis is linked to the decomposition of lignin, characterized by a gradual loss of mass where DTG tends towards zero from 400 °C.

4.3. Thermal Analysis

Figure 9 shows the evolution of temperatures in SARP for stages II, III and IV of the experiment, as well as the behavior of Direct Normal Irradiance (DNI).

Stage II begins with the aperture of the solar furnace shutter During this period, it is observed that reactor temperatures increase rapidly. T_{rec} increases from an ambient temperature of ~30 °C to 900 °C in 8 min. During experimentation, the shutter was kept fully open, stabilizing the air temperature at the volumetric receiver outlet at 947 °C for

130 min. Stage II is concluded when a threshold temperature (T_{intMax}) of 600 °C is reached after 37 min, however it depends on irradiance conditions.

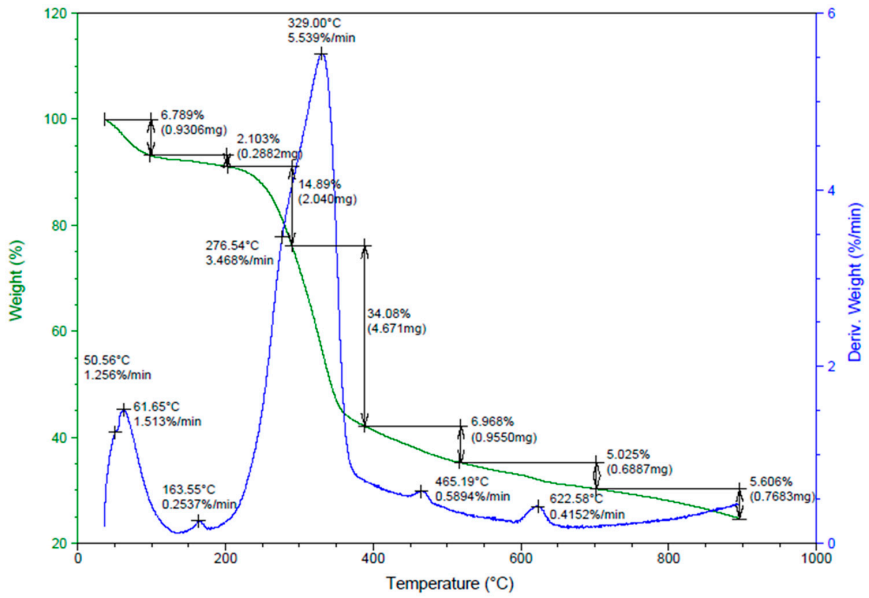


Figure 8. TGA and DTG analysis of the *Carya illinoinensis* pruning.

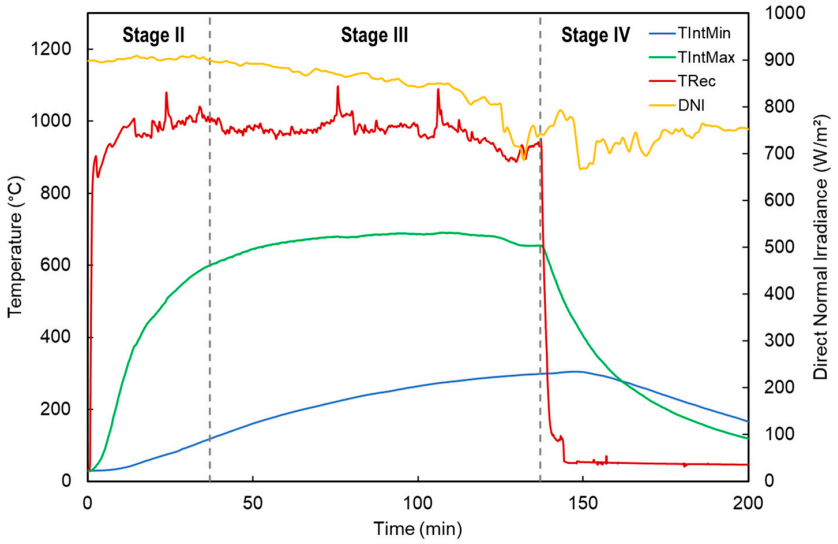


Figure 9. Evolution of temperatures in stages II, III and IV, and DNI data. The combined uncertainty is approximately 1.32 °C, calculated using a coverage factor of k = 2 [33].

Stage III initiates the movement of the screw leading to the displacement of organic matter within the reactor. During experimentation the average temperature in the pyrolysis zone was T_{IntMax} = 669 °C ± 21, while the temperature of the porous media (T_{rec}) remained at 970 °C ± 30, in addition DNI had an average value of 848 W/m^2 ± 49. The output of synthesis gas was observed at approximately t = 40 min.

T_{Rec} behavior is influenced by the adjustment of the heliostat tracking system during operation. The temperature values recorded at this point vary with respect to the peak positioning of the concentrated solar radiation received by the volumetric receiver. However, because adjustments are made at short intervals, there is no significant change in the temperatures inside the reactor.

The heating method of this reactor is one of the most distinctive characteristics. In this system, the flow of thermal energy arrives from one of the longitudinal ends of the

reactor, i.e., from one of the bases of the cylinder. In contrast, in previously reported Auger reactors where heating comes from the longitudinal center or at a point very close to it. For this reason, the determination of the temperature distribution throughout the reactor is considered important for the performance of the pyrolysis reaction.

Figure 10 shows the behavior of reactor surface temperatures (T_0, T_1, T_2 and T_3) as a function of reactor length for time intervals of 20 min. Figure 10a exhibits the temperature curves for stages II and III, corresponding to the heating phase. On the other hand, Figure 10b shows the temperatures of stage IV, which correspond to the cooling of the SARP.

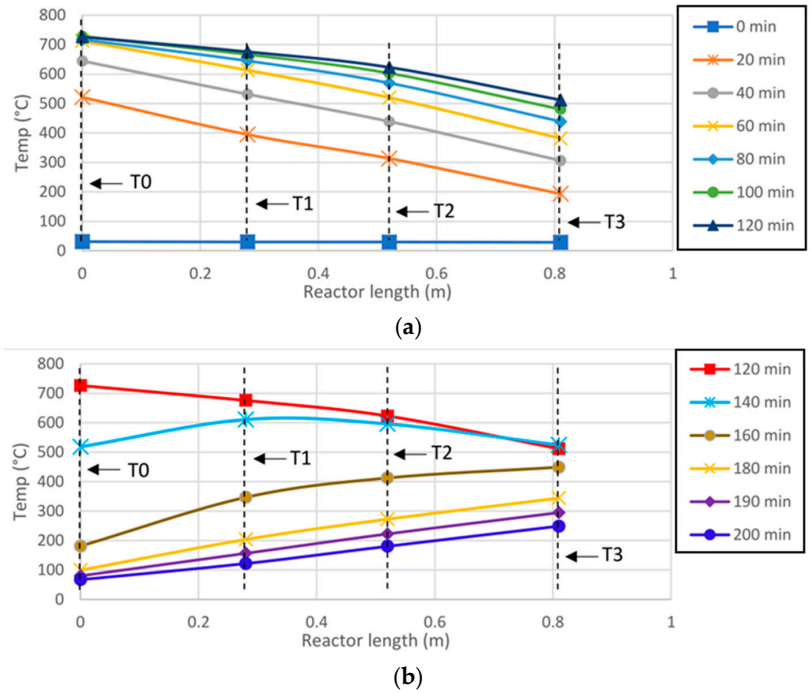


Figure 10. Temperature distribution profile as a function of reactor length in 20 min time intervals. (**a**) Heating process: Stages II and III and (**b**) Cooling process: Stage IV.

The initial reactor temperature is 29.9 °C (blue line), and after 20 min of starting heating (orange line), the thermocouple T_0, reaches a temperature of 500 °C, while the thermocouple T_3 shows 200 °C, just 0.8m from the front of the SARP obtaining a temperature gradient of 300 °C between the frontal and rear part of the reactor. As the reactor heats up and after 120 min of heating, this temperature difference decreases to 200 °C (Figure 10a).

The gray line represents the temperatures recorded at the onset of the pyrolysis process. At this stage, the value of T_0 is similar to that of T_{IntMax}, with a percentage difference of 5.1%. On the other hand, the percentage difference between T_3 and T_{IntMin} is 81%. Although the 306 °C recorded at T_3 is sufficient to initiate pyrolysis, this temperature is only reached at T_{IntMin} after 150 min, corresponding to Stage IV.

From 60 min onward, the temperatures at T_0 and T_1 approach steady state, remaining within the operating limits of the reactor materials (<750 °C). In contrast, T_2 reaches steady state only after 100 min, while T_3 requires more than 140 min under the same irradiance conditions.

Figure 10b presents the cooling behavior of the SARP during Stage IV. The receiver shows a sharp temperature decrease at T_0, with a 33.3% drop between 120 and 140 min, but the largest temperature decrease (96.6%) appears between 140 and 160 min. Due to their greater distance from the receiver, T_1 and T_2 exhibit reductions of 55.1% and 36.3% in the same interval, respectively.

After 160 min, the thermal behavior of the SARP's frontal zone is reversed, with T_0 becoming the coldest point in the reactor. This inversion occurs because the volumetric receiver no longer absorbs concentrated solar radiation, while the reactor body remains hot; consequently, the temperatures at T_1, T_2, and T_3 exceed that of T_0.

4.4. Hydrogen Production

During the first experimental campaign, hydrogen production was monitored as an indicator of the pyrolysis process. Figure 11 shows the H_2 concentration (% vol) measured by gas chromatography and its relationship with the internal reactor temperatures, T_{IntMin} and T_{IntMax}.

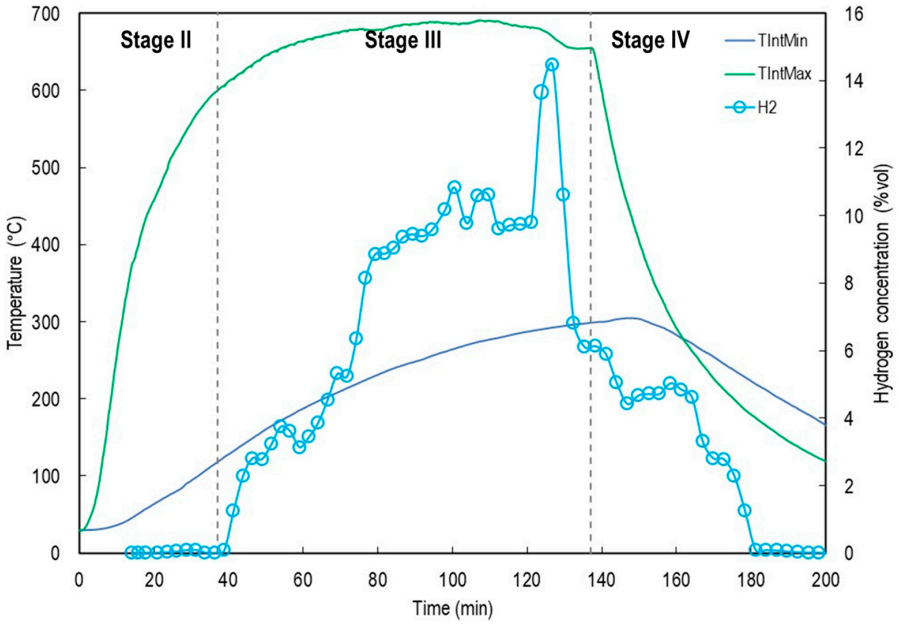


Figure 11. Evolution of temperatures and hydrogen production.

As illustrated in Figure 11, hydrogen production exhibited a strong correlation with reactor temperature, particularly with the average value of T_{IntMax}. Following the activation of the feeding screw, the H_2 concentration increased sharply, reaching peak values between 2.5 and 3.0% vol. during the thermal steady-state phase. These results confirm that the pyrolytic decomposition of walnut tree pruning under solar heating produces both condensable and non-condensable volatiles, while also promoting hydrogen formation, likely through secondary cracking and reforming reactions.

As shown in the graph, hydrogen production began with the opening of the attenuator (Stage III) and continued for 148 min, reaching a peak concentration of 14.5% vol 88 min after the onset of pyrolysis. Hydrogen generation continued even after the attenuator was closed, during the cooling phase (Stage IV), for an additional 43 min. During this period, the maximum and minimum average reactor temperatures were T_{IntMax} = 345 °C and T_{IntMin} = 278 °C, respectively. Moreover, the highest temperature recorded at the coldest point inside the reactor during Stage IV was 305 °C, measured 11 min after attenuator closure. This temperature was sufficient to sustain pyrolysis reactions within the bed formed beneath the feeding screw, composed of fine particles (<4 mm) that were not transported forward.

4.5. Biochar

Under the analyzed experimental conditions, a biochar yield of 65.08% (wet/ash basis) was obtained for a residence time of ~100 min. Although a high yield of biochar is favored

by shorter residence times, the non-uniform temperature distribution within the reactor influences this yield. T_{IntMax} measures the highest temperature of raw material; however, organic matter moves through lower temperature zones as recorded by T_{IntMin}, obtaining an incomplete biomass transformation. These results are comparable with the yields obtained by Kakku et al. [34], who reported a 53% conversion to biochar for a temperature of 400 °C in a screw reactor with a similar raw material according to the reported proximate and ultimate analyses. Furthermore, Syafiqah et al. [35] reported the pyrolysis of a biomass with physicochemical properties similar to those in this study in a fixed-bed reactor using Fresnel lens technology, achieving a biochar yield of 32% (dry, ash-free basis) at 435 °C.

The XRD analysis of the biochar indicated the following crystalline phases: C in graphite form, $CaSO_4$, $CaCO_3$, $CaC_2O_4 \cdot H_2O$ and $CaMnF_5$. On the other hand, the identification of $CaSO_4$ and $CaCO_3$ indicates mineral impurities commonly found in agro-industrial wastes and formed by reacting with SO_2 and CO_2, respectively. Additionally, $CaC_2O_4 \cdot H_2O$ is a compound frequently found in walnut shells (which is the fruit of the *Carya illinoinensis* tree) and can be detected after thermal processes if not fully decomposed. Finally, $CaMnF_5$ indicates possible interactions of raw material with some reactor components.

The results of the SEM analysis of biochar are shown in Figure 12. The morphology of *Carya illinoinensis* surface before pyrolysis is observed in Figure 12a. The thermal decomposition accelerates the structural composition of *Carya illinoinensis* obtaining an amorphous structure with pores and cracks (Figure 12b). On the other hand, in Figure 12c prismatic structures corresponding to mineral crystalline phases are observed on the surface.

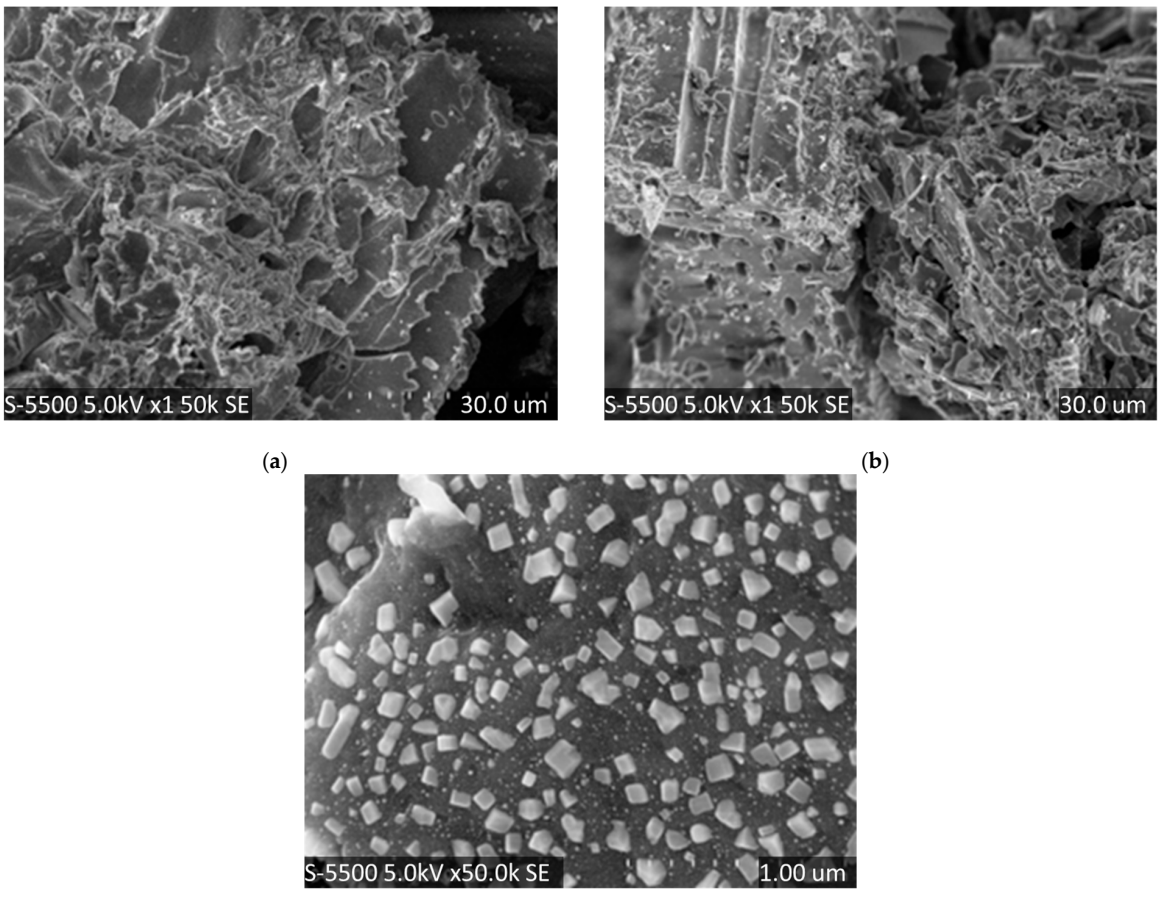


Figure 12. Morphology of (**a**) *Carya illinoinensis* pruning at 500×, (**b**) *Carya illinoinensis* pruning biochar at 500× and (**c**) *Carya illinoinensis* pruning biochar at 50,000×.

5. Discussion

The results obtained from the solar-driven pyrolysis experiments demonstrate the technical feasibility of operating a solarized auger reactor under real operating conditions for the conversion of agricultural biomass into hydrogen-rich syngas. The thermal and chemical response of the system reveals critical insights into reactor performance, dynamic process, and solar integration.

5.1. Thermal Behavior and Reactor Stability

Figure 9 illustrates the ability of the reactor to reach and maintain the high temperatures required for effective pyrolysis. Under stable solar irradiance input, the temperature at the volumetric receiver exceeded 1000 °C, while the internal pyrolysis zone (T_{IntMax}) stabilized around 620–650 °C. This range is consistent with literature-reported optimal temperatures for fast pyrolysis and gas-phase cracking of volatiles. However, a significant axial temperature gradient was observed, with T_{IntMin} remaining around 300 °C, suggesting non-uniform heat distribution along the reactor length. This gradient is characteristic of solar-irradiated systems with unidirectional energy input.

The behavior of T_{Rec} was found to be influenced by several factors, mainly by fluctuations in direct normal irradiance and adjustments in the heliostat tracking system. The latter produces variations in temperature due to the changes in the position of the solar flux peak received by the volumetric receiver. However, since such adjustments were performed at short intervals, no significant effects were observed on the internal reactor temperatures. This highlights the thermal stability of the SARP under variable solar conditions.

5.2. Longitudinal Temperature Distribution Profile

The longitudinal temperature distribution profile on the reactor surface proved to be a key factor for pyrolysis performance. A minimum temperature of 300 °C was identified as necessary to promote thermal degradation of biomass components. Although only surface temperatures were recorded, they provide a valuable approximation of the internal reaction environment, serving as a reference for future studies on longitudinally heated reactors. Interestingly, the expected exponential distribution was not observed. Instead, both heating and cooling curves exhibited nearly linear trends (Figure 11), which has important implications for modeling heat transfer phenomena during solar pyrolysis. These results suggest that reactor design and thermal inertia contribute to a more homogeneous temperature distribution than initially assumed.

Another limitation identified was the impossibility of directly measuring the actual reaction temperature. Only approximations from T_{IntMax} readings were available. Nevertheless, the thermal behavior observed offers a basis for future correlations between surface and internal temperatures, which could support improved reactor monitoring and operational protocols.

5.3. Biochar Production

As noted in Section 4.5, the high biochar yield results from incomplete pyrolysis, strongly influenced by the non-uniform temperature distribution and the internal Archimedes screw. Figures 9 and 10 show that the internal thermocouples record markedly different temperatures: T_{IntMin}, near the feeding zone, averages 232.6 °C, while T_{IntMax}, near the focal zone, averages 669 °C, yielding a gradient of 436.4 °C across the reactor. Although the slow screw movement favors gradual heating, heat transfer limitations constrain temperature rise.

To improve mixing and extend residence time, paddles were integrated between the flights of the auger shaft in the first half of the screw (Figure 5b). These paddles redirect part

of the biomass backward, delaying its advance and avoiding immediate exposure to higher-temperature regions. Consequently, partially pyrolyzed material mixes with unreacted feedstock, leading to non-uniform conversion and higher biochar yield compared with more controlled pyrolysis systems.

Due to equipment limitations, conversion rates could not be quantified. Future work will address pyrolysis conversion and the role of temperature distribution in product selectivity.

5.4. Hydrogen Production and Pyrolysis Dynamics

Several experimental studies have reported hydrogen generation during biomass pyrolysis under different operating conditions. Alvarado documented peak hydrogen yields as a function of temperature for various feedstock, finding that maximum production generally occurs above 700 °C [36]. Xia investigated the pyrolysis of Chinese chestnut shells and showed that H_2 production increases with temperature, both in the absence and presence of a catalyst, with maximum yields reached at 800 °C [37]. Al Arni compared slow and fast pyrolysis of sugarcane bagasse, demonstrating that the heating rate has a direct proportional effect on hydrogen generation [38].

In this work, the fluctuations observed in H_2 production (Figure 11) can be explained by the progressive transport of biomass by the screw conveyor, which exposes the material to zones of increasing temperature along the reactor. This dynamic results in a gradual increase in heating rate, thereby inducing oscillations in hydrogen generation. Such findings underscore the relevance of residence time control and heating profiles in continuous solar-driven pyrolysis.

5.5. Process Relevance and Technological Outlook

From a technological perspective, the solar Auger reactor demonstrated clear advantages for continuous biomass processing with direct solar heat. Compared to batch systems, this configuration allows precise control of residence time, mixing, and feed rate, all of which are essential for process scalability. Furthermore, the use of agro-industrial residues such as walnut pruning waste illustrates the potential of solar pyrolysis to contribute to a circular and decarbonized economy by producing both green hydrogen and biochar.

Despite these promising outcomes, several challenges remain. The thermal gradient along the reactor must be minimized to achieve more uniform conversion. Longer and more stable irradiation periods should be tested to evaluate process performance under near-industrial conditions. In addition, systematic studies on product yields and composition (gas, liquid, and solid) under varying operational parameters are required to optimize process efficiency and strengthen the technological readiness of solar-driven pyrolysis.

6. Conclusions

The experimental evaluation of a solarized Auger-type reactor for pyrolysis, named SARP, designed to operate under real direct solar irradiation conditions, has demonstrated its potential for continuous high-temperature (700 °C) biomass pyrolysis. The process produced biochar with a yield of 65.1% and synthesis gas containing hydrogen at concentrations relevant for energy applications.

During pyrolysis, average steady-state reactor temperatures of 669 °C ± 21 were achieved, along with sustained hydrogen production for 148 min, reaching a peak concentration of 14.5% vol at 88 min. Additionally, synthesis gas was generated at the onset of the cooling phase, during the 43 min following attenuator closure. These results confirm the feasibility of using concentrated solar energy to drive the thermochemical conversion of agricultural residues.

Temperature fluctuations in the volumetric receiver, measured by the T_{Rec} thermocouple and caused by adjustments to the optical system or cloud cover, were imperceptible inside the reactor as recorded by T_{IntMin} and T_{IntMax} over the short term. This demonstrates the system's high resilience to radiative fluctuations under real operating conditions, attributable to its high thermal inertia and low axial temperature gradients in the critical zones of the SARP.

Future efforts should focus on optimizing the flux distribution in the receiver and increasing axial temperature uniformity within the reactor, without reducing the maximum temperatures recorded by T_{IntMax}. Additionally, hybrid control strategies are needed to ensure process stability and scalability. These findings contribute to the development of sustainable solar technologies for decentralized hydrogen and biofuel production in regions with abundant biomass from agro-industrial processes and high direct solar radiation.

7. Patents

The reactor system presented in this study is the subject of an ongoing patent application.

Author Contributions: Conceptualization, E.A.R., N.A.C.-C., P.P.M. and C.A.E.; methodology, E.A.R. and A.A.-M.; software, E.A.R. and A.A.-M.; validation, H.I.V.V. and C.A.E.; formal analysis, E.A.R., N.A.C.-C., A.A.-M. and H.I.V.V.; investigation, E.A.R., N.A.C.-C. and C.A.E.; resources, C.A.E.; data curation, E.A.R. and A.A.-M.; writing—original draft preparation, E.A.R. and N.A.C.-C.; writing—review and editing, E.A.R., N.A.C.-C., A.A.-M. and H.I.V.V.; visualization, C.A.E.; supervision, C.A.E.; project administration, C.A.E.; funding acquisition, C.A.E. All authors have read and agreed to the published version of the manuscript.

Funding: The authors gratefully acknowledge the support of the Secretaría de Ciencia, Humanidades, Tecnología e Innovación (SECIHTI) for the postdoctoral fellowship carried out at the Institute of Renewable Energies by the researcher Ernesto Anguera-Romero with CVU: 378009. The authors also express their gratitude to project DGAPA-UNAM PAPIIT-AG101525 for providing the financial support that made this work possible.

Data Availability Statement: The data supporting the findings of this study are not publicly available at this time as they involve results from a preliminary study related to a patent application and intellectual property protection. Data may be made available by the corresponding author upon reasonable request, once the patenting process has been completed.

Acknowledgments: The authors acknowledge the technical support of María del Rocío Nava Lara, María Luisa Ramón for the XRD analysis, Patricia Altuzar for the TGA, and Rogelio Elvira Morán for the SEM analysis. During the preparation of this manuscript/study, the authors used Parts of this manuscript were translated and refined using an AI-based translation tool (ChatGPT-5, developed by OpenAI, San Francisco, CA, USA) to improve clarity and accuracy in English. The authors have reviewed and edited the output and take full responsibility for the content of this publication.

Conflicts of Interest: Author Pablo Pizarro-Medina was employed by the company Green Oil Energy Systems SLP. The remaining authors declare that the research was conducted in the absence of any commercial or financial relationships that could be construed as a potential conflict of interest.

Abbreviations

The following abbreviations are used in this manuscript:

SARP	Solarized Auger Reactor for Pyrolysis
IER-UNAM	Instituto de Energías Renovables—Universidad Nacional Autónoma de México
GHG	Green House Gas
DGAPA	Dirección General de Asuntos Académicos (General Directorate of Academic Affairs)

PAPIIT	Programa de Apoyo a Proyectos de Investigación e Innovación Tecnológica (Support Program for Research and Technological Innovation Projects)
HoSIER	Horno Solar (Solar Furnace) del Instituto de Energías Renovables
DNI	Direct Normal Irradiance
HHV	Higher Heating Value
TGA	Thermogravimetric Analysis
T_{IntMin}	Minimum Internal Temperature
T_{IntMax}	Maximum Internal Temperature
T_{Rec}	Volumetric Receiver Temperature

References

1. Altundoğan, H.S.; Tanyıldızı, M.Ş.; Kalender, M.; Elçiçek, S.; Pehlivan, D. A novel screw-type pyrolysis system for selectively producing value-added chemicals from lignocellulosic biomass. *Biomass Convers. Biorefinery* **2025**, *15*, 9193–9204. [CrossRef]
2. Wang, G.; Dai, Y.; Yang, H.; Xiong, Q.; Wang, K.; Zhou, J.; Li, Y.; Wang, S. A Review of Recent Advances in Biomass Pyrolysis. *Energy Fuels* **2020**, *34*, 15557–15578. [CrossRef]
3. Wang, J.; Wang, S. Preparation, modification and environmental application of biochar: A review. *J. Clean. Prod.* **2019**, *227*, 1002–1022. [CrossRef]
4. Xiu, S.; Shahbazi, A. Bio-oil production and upgrading research: A review. *Renew. Sustain. Energy Rev.* **2012**, *16*, 4406–4414. [CrossRef]
5. Lee, S.; Tsang, Y.F.; Lin, K.-Y.A.; Kwon, E.E.; Lee, J. Employment of biogas as pyrolysis medium and chemical feedstock. *J. CO2 Util.* **2022**, *57*, 101877. [CrossRef]
6. Winter, C.L.; Sizmann, R.L.; Vant-Hull, L.L. *Solar Power Plants*, 1st ed.; Springer: Berlin/Heidelberg, Germany, 1991. [CrossRef]
7. Campuzano, F.; Brown, R.C.; Martínez, J.D. Auger reactors for pyrolysis of biomass and wastes. *Renew. Sustain. Energy Rev.* **2019**, *102*, 372–409. [CrossRef]
8. Kapoor, L.; Bose, D.; Mekala, A. Biomass pyrolysis in a twin-screw reactor to produce green fuels. *Biofuels* **2020**, *11*, 101–107. [CrossRef]
9. Zhou, C.; Zhang, Y.; Liu, Y.; Deng, Z.; Li, X.; Wang, L.; Dai, J.; Song, Y.; Jiang, Z.; Qu, J.; et al. Co-pyrolysis of textile dyeing sludge and red wood waste in a continuously operated auger reactor under microwave irradiation. *Energy* **2021**, *218*, 119398. [CrossRef]
10. Álvarez-Chávez, B.J.; Godbout, S.; Raghavan, V. Optimization of microwave-assisted hydrothermal pretreatment and its effect on pyrolytic oil quality obtained by an auger reactor. *Biofuel Res. J.* **2021**, *8*, 1316–1329. [CrossRef]
11. Ferreira, S.D.; Manera, C.; Silvestre, W.P.; Pauletti, G.F.; Altafini, C.R.; Godinho, M. Use of Biochar Produced from Elephant Grass by Pyrolysis in a Screw Reactor as a Soil Amendment. *Waste Biomass Valorization* **2019**, *10*, 3089–3100. [CrossRef]
12. Salgado, M.A.H.; Coba, S.J.A.; Tarelho, L.A. Simultaneous production of biochar and thermal energy using palm oil residual biomass as feedstock in an auto-thermal prototype reactor. *J. Clean. Prod.* **2020**, *266*, 121804. [CrossRef]
13. Lugovoy, Y.V.; Chalov, K.V.; Tarabanko, V.E.; Stepacheva, A.A.; Kosivtsov, Y.Y. Fast Pyrolysis of Flax Shive in a Screw-Type Reactor. *Chem. Eng. Technol.* **2021**, *44*, 2056–2063. [CrossRef]
14. Promdee, K.; Vitidsant, T. Industrial single-screw and twin-screw prototype reactor pyrolysis for bio-oil and charcoal production from biomass: A case study of cogon grass (*Imperata cylindrica*). *Results Eng.* **2025**, *26*, 104585. [CrossRef]
15. Kapoor, L.; Mohammad, A.; Jha, J.M.; Srivastava, N.; Jana, S.K.; Alshahrani, M.Y.; Ahmad, I.; Pal, D.B.; Gupta, V.K. Biofuel production using fast pyrolysis of various plant waste biomasses in fixed bed and twin-screw reactors. *Int. J. Energy Res.* **2022**, *46*, 19278–19286. [CrossRef]
16. Ayyadurai, S.; Arunachalam, K.D. Experimental investigations on sugarcane bagasse pyrolytic oil production from flash pyrolysis using a rotary screw reactor. *Biofuels Bioprod. Biorefining* **2022**, *16*, 576–586. [CrossRef]
17. Solar, J.; Caballero, B.M.; López-Urionabarrenechea, A.; Acha, E.; Arias, P.L. Pyrolysis of Forestry Waste in a Screw Reactor with Four Sequential Heating Zones: Influence of Isothermal and Nonisothermal Profiles. *Ind. Eng. Chem. Res.* **2021**, *60*, 18627–18639. [CrossRef]
18. Qin, L.; Shao, Y.; Hou, Z.; Jiang, E. Effect of temperature on the physicochemical characteristics of pine nut shell pyrolysis products in a screw reactor. *Energy Sources Part A Recov. Util. Environ. Eff.* **2020**, *42*, 2831–2843. [CrossRef]
19. Mandal, S.; Haydary, J.; Bhattacharya, T.K.; Tanna, H.R.; Husar, J.; Haz, A. Valorization of Pine Needles by Thermal Conversion to Solid, Liquid and Gaseous Fuels in a Screw Reactor. *Waste Biomass Valorization* **2019**, *10*, 3587–3599. [CrossRef]
20. Xu, T.; Xu, J.; Wu, Y. Hydrogen-Rich Gas Production from Two-Stage Catalytic Pyrolysis of Pine Sawdust with Calcined Dolomite. *Catalysts* **2022**, *12*, 131. [CrossRef]
21. Bartolucci, L.; Cordiner, S.; Mele, P.; Mulone, V. Defatted spent coffee grounds fast pyrolysis polygeneration system: Lipid extraction effect on energy yield and products characteristics. *Biomass Bioenergy* **2023**, *179*, 106974. [CrossRef]

22. Zolfagharpour, H.R.; Sharafati, A.; Hosseinzadeh, M. Effect of V_2O_5 nanoparticles and temperature on the chemical compounds of bio-oils in catalytic pyrolysis of sugarcane bagasse. *Biomass Convers. Biorefinery* **2024**, *14*, 19479–19488. [CrossRef]
23. Ünsaç, A.; Okutan, H.C.; Karatepe, N. Low tar yield and high energy conversion efficiency in a continuous pyrolysis reactor with modified ribbon screw conveyor. *Int. J. Hydrogen Energy* **2024**, *53*, 1332–1343. [CrossRef]
24. Abnisa, F.; Daud, W.M.A.W. A review on co-pyrolysis of biomass: An optional technique to obtain a high-grade pyrolysis oil. *Energy Convers. Manag.* **2014**, *87*, 71–85. [CrossRef]
25. Maytorena, V.; Buentello-Montoya, D. Worldwide developments and challenges for solar pyrolysis. *Heliyon* **2024**, *10*, e35464. [CrossRef]
26. Zavattoni, S.A.; Montorfano, D.; Good, P.; Ambrosetti, G.; Barbato, M.C. The synhelion absorbing gas solar receiver for 1'500 °C process heat: CFD modeling. In Proceedings of the SOLARPACES 2019: International Conference on Concentrating Solar Power and Chemical Energy Systems, Daegu, Republic of Korea, 1–4 October 2019; p. 030037. [CrossRef]
27. Zeng, K.; Gauthier, D.; Li, R.; Flamant, G. Solar pyrolysis of beech wood: Effects of pyrolysis parameters on the product distribution and gas product composition. *Energy* **2015**, *93*, 1648–1657. [CrossRef]
28. Aspiazu-Méndez, A.; Cisneros-Cárdenas, N.A.; Pérez-Rábago, C.; Pat-Espadas, A.M.; Manzini-Poli, F.; Estrada, C.A. Analysis of the Solar Pyrolysis of a Walnut Shell: Insights into the Thermal Behavior of Biomaterials. *Energies* **2024**, *17*, 1435. [CrossRef]
29. *ASTM E870-82*; Standard Test Methods for Analysis of Wood Fuels. ASTM International: West Conshohocken, PA, USA, 2019.
30. *ISO 17828:2015*; Solid Biofuels—Determination of Bulk Density. International Organization for Standardization: Geneva, Switzerland, 2015.
31. Channiwala, S.; Parikh, P. A unified correlation for estimating HHV of solid, liquid and gaseous fuels. *Fuel* **2002**, *81*, 1051–1063. [CrossRef]
32. Sluiter, A.; Hames, B.; Ruiz, R.; Scarlata, C.; Sluiter, J.; Templeton, D. *Determination of Ash in Biomass: Laboratory Analytical Procedure (LAP)*; Technical Report NREL/TP-510-42622; National Renewable Energy Laboratory: Golden, CO, USA, 2008.
33. Farrance, I.; Frenkel, R. Uncertainty of Measurement: A Review of the Rules for Calculating Uncertainty Components through Functional Relationships. *Clin. Biochem. Rev.* **2012**, *33*, 49–75. [PubMed] [PubMed Central]
34. Kakku, S.; Naidu, S.; Bhatt, M.; Chakinala, A.G.; Joshi, J.; Gautam, S.; Mohanty, K.; Kataria, G.; Sharma, A. Pyrolytic conversion of agricultural residue using continuous auger reactor for resource recovery. *J. Anal. Appl. Pyrolysis* **2023**, *171*, 105951. [CrossRef]
35. Abdul Hamed, A.S.; Yahya, M.S.; Abdul Latiff, N.A.; Ma'arif, S.; Munajat, N.F. Solar Pyrolysis of Empty Fruit Bunch (EFB): Biochar Characterization and Potential Applications. *J. Adv. Res. Fluid Mech. Therm. Sci.* **2025**, *133*, 185–194. [CrossRef]
36. Alvarado-Flores, J.J.; Alcaraz-Vera, J.V.; Ávalos-Rodríguez, M.L.; Guzmán-Mejía, E.; Rutiaga-Quiñones, J.G.; Pintor-Ibarra, L.F.; Guevara-Martínez, S.J. Thermochemical Production of Hydrogen from Biomass: Pyrolysis and Gasification. *Energies* **2024**, *17*, 537. [CrossRef]
37. Xia, S.; Li, K.; Xiao, H.; Cai, N.; Dong, Z.; Xu, C.; Chen, Y.; Yang, H.; Tu, X.; Chen, H. Pyrolysis of Chinese chestnut shells: Effects of temperature and Fe presence on product composition. *Bioresour. Technol.* **2019**, *287*, 121444. [CrossRef] [PubMed]
38. Al Arni, S. Comparison of slow and fast pyrolysis for converting biomass into fuel. *Renew. Energy* **2018**, *124*, 197–201. [CrossRef]

Disclaimer/Publisher's Note: The statements, opinions and data contained in all publications are solely those of the individual author(s) and contributor(s) and not of MDPI and/or the editor(s). MDPI and/or the editor(s) disclaim responsibility for any injury to people or property resulting from any ideas, methods, instructions or products referred to in the content.